Statistical Properties of Carbon Nanostructures

Forrest H. Kaatz, Mesalands Community College, Tucumcari, NM, USA
Adhemar Bultheel, Dept. Computer Sci., KU Leuven, Heverlee, Belgium

Abstract

We look at modeling carbon nanostructures from a theoretical graph network view, where a graph has atoms at a vertex and links represent bonds. In this way, we can calculate standard statistical mechanics functions (entropy, enthalpy, and free energy) and matrix indices (Wiener Index) of finite structures, such as fullerenes and carbon nanotubes. The Euclidean Wiener Index (topographical index) is compared with its topological (standard) counterpart. For many of these parameters, the data have power law behavior, especially when plotted versus the number of bonds or the number of atoms. The number of bonds in a carbon nanotube is linear with the length of the nanotube, thus enabling us to calculate the heat of formation of capped (5,5) and (10,10) nanotubes. These properties are determined from atomic coordinates using MATLAB routines.

Keywords: fullerenes; carbon nanotubes; statistical mechanics; Wiener index; MATLAB

1 Introduction

Carbon has many allotropes (diamond, graphite, fullerenes, and carbon nanotubes, (CNTs)) that illustrate the amazing chemical and structural diversity of element number six. We consider the nanosized forms in our calculations; fullerenes and CNTs. Fullerenes were discovered in 1985 [1], carbon nanotubes in 1991 [2], and graphene in 2004 [3]. As a result of these groundbreaking discoveries, there are now literally thousands of scientists studying novel forms of carbon and their properties.

The first fullerene to be discovered was C_{60}, with a structure described as similar to that of a football (soccer ball) [1] with pentagonal cycles separated by hexagonal ones, see Figure 1A. This so-called isolated pentagon rule (IPR) is thought to stabilize the fullerene structure, since pentagonal bonds cost more energy than hexagonal ones [4]. Thus, pentagonal cycles are found separated by hexagonal ones, so that there is 26 maximum separation between the two types. The smallest fullerene is C_{20}, consisting of 12 pentagons. In general, a fullerene has n 3-valent vertices with 12 pentagons and $(n/2 - 10)$ hexagons, with $3/2n$ carbon-carbon bonds [5,6]. Experimentally, there is evidence of fullerenes as large as C_{418}, found in soot [7]. There are many isomers of the fullerene structures, so that several possible structures exist; however, most of these are not favored energetically

Nanotubes were discovered in 1991 [2], as straight 'helical' coils of carbon, although filamentous carbon [8] was known prior to 1991. Thus a nanotube can be thought of as a rolled up sheet of graphene, with hemispheres of fullerenes at the ends. A commonly accepted growth mechanism [9,10] is that nanotubes form by catalytic action of transition metals, such as iron or cobalt, with a cap at one end and the open growth end eventually becoming closed after some aspect ratio is created. The nanotube analogue to C_{60}, the most common fullerene, seems to be a (10,10) nanotube capped with hemispheres of C_{240} [10], see Figure 1B and 1C.

Nanotubes are defined [11] by their 'chiral vector', or angle cut through the 2D layer of graphene, with

$$n\mathbf{a}_1 + m\mathbf{a}_2 \equiv (n, m) \tag{1}$$

where the indices (n, m) describe the number of unit vectors in the hexagonal graphene honeycomb lattice. There are two common geometries, a 'zigzag' nanotube, with a chiral angle of $\theta = 0°$, and an 'armchair' nanotube with $\theta = 30°$, leaving a general chiral nanotube with $0° \leq \theta \leq 30°$. The chiral angle is given by:

$$\theta = \tan^{-1}\left[\sqrt{3}m/(m + 2n)\right] \tag{2}$$

and the nanotube diameter is

$$d_t = C_h/\pi = \sqrt{3}a_{c-c}(m^2 + mn + n^2)^{1/2}/\pi \tag{3}$$

where a_{c-c} is the carbon-carbon nearest neighbor distance (1.421 Å) in graphite. Thus the (10,10) nanotube is of the armchair variety.

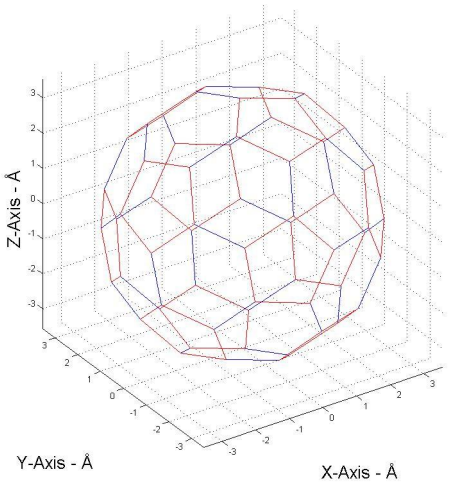

A. MATLAB plot of $C_{60}(I_h)$. Contrast indicates pentagonal cycles in the structure.

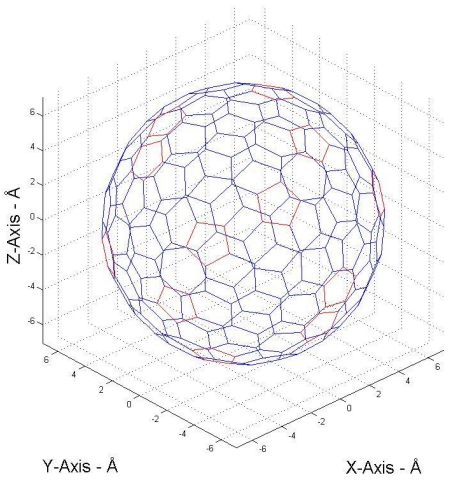

B. MATLAB plot of $C_{240}(5v)$. Contrast indicates pentagonal cycles in the structure.

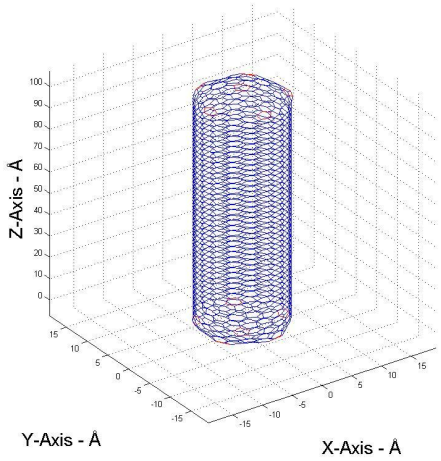

C. MATLAB plot of carbon nanotube (10,10) 100 Å

Figure 1: MATLAB plots

2 Methods

We employ a graph-theoretical approach, where nodes represent atoms, and an edge represents a bond between sites, $G = (V, E)$. We create a graph of the nanosized form of carbon by creating bonds (links) between nearest neighbors up to 1.3 times the shortest neighbor distance. These vary from 20 to 8360 atoms for fullerenes and nanotubes. An adjacency matrix is created and may exist in two forms. The standard form [12] is

$$A = \begin{cases} H(r_c - r_{ij}) & i \neq j \\ 0 & i = j \end{cases} \tag{4}$$

where the Heaviside step function $H(r_c - r_{ij}) = 1$ if $r_c < 1.3$**shortest distance to r_{ij}), and i and j represent atomic sites, and r_c is the cutoff value. Alternatively, we may consider the actual Euclidean distances in the adjacency matrix [13,14], so that $H(r_c – r_{ij}) = e_{ij}$, the Euclidean distance between atoms.

The approach to modeling the free energy, enthalpy, and entropy has been discussed in the literature [15,16]. These can all be determined from the appropriate adjacency matrix. We also calculate one of the oldest indices, the Wiener index [17], as

$$W = \frac{1}{2} \sum_{i=1}^{N} \sum_{j=1}^{N} d_{ij} \tag{5}$$

where N is the number of atoms and d_{ij} is the shortest path distance between atoms i and j. In the standard form, the distances between atoms = 1, and in the Euclidean form [13], it is e_{ij}, so that we calculate W_E, the Euclidean 3D Wiener index. The collection of data starts from the atomic coordinates, and proceeds to calculating the adjacency matrix, and from it, all the results come from one MATLAB routine.

3 Results

In Figure 1, we show plots of finite nanocarbons, $C_{60}(I_h)$, $C_{240}(5v)$, and a (10,10) nanotube. In our notation, the fullerene isomers are listed in parentheses as I_h or $5v$. The fullerenes and nanotubes have atoms with 3-fold coordination and the hexagonal and pentagonal cycles are shown in blue and red respectively. Once we have created the adjacency matrix, the statistical mechanics data can be calculated [15,16]. The partition function is:

$$Z(G, \beta) = \mathrm{Tr}(e^{\beta A})$$

where A is the adjacency matrix for the graph G, and $\beta = 1/(k_B T)$. At $T = 300K$, we have $\beta = 38.68173/eV$. The entropy can be determined as

$$S(G, \beta) = -k_B \sum_j \lambda_j p_j + k_B \ln(Z) \sum_j p_j$$

where λ_j is an eigenvalue of A and

$$p_j = \frac{e^{\beta \lambda_j}}{Z(G, B)}$$

is the probability that the ensemble occupies a microstate j. The free energy is the natural logarithm of the partition function,

$$F(G, \beta) = -\frac{\ln Z(G, \beta)}{\beta}$$

and the enthalpy can be defined as follows:

$$H(G, \beta) = -\frac{1}{Z(G, \beta)} \mathrm{Tr}(A e^{\beta A}).$$

We then plot the free energy, enthalpy, and entropy, per bond, versus the number of bonds in the nanocarbons. This results in plots with good power law [18] regression statistics as shown in Figure 2. We plot the data/bond versus the number of bonds for fullerenes and nanotubes. The distinction between (a) and (b) is that in (a), we have used an adjacency matrix with Euclidean distances, and in (b), we have used the standard adjacency matrix with zeros and ones. The bestfit equations in (a) have different leading coefficients, so that the entropy and enthalpy coincide (neglecting the sign difference) for small ($\approx$ 100 atoms) nanocarbons, and since the slope is different, the plots diverge for larger structures. These quantities are divided by the number of bonds in the nanocarbon and plotted versus N_B, to give a power law plot. The asymptote of zero for large N_B makes intuitive sense, since if we imagine the data/bond is finite, then as the number

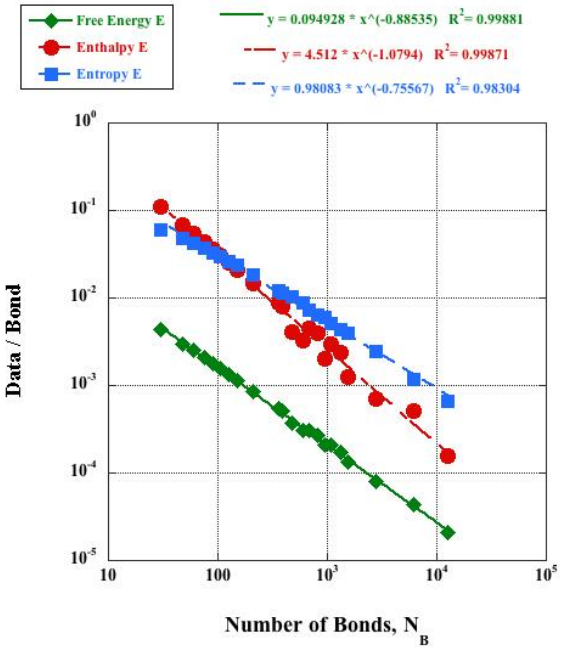

(a) Plots of the free energy, enthalpy, and entropy / bond versus the number of bonds. The data clearly exhibits power law character. This plot uses a Euclidean adjacency matrix.

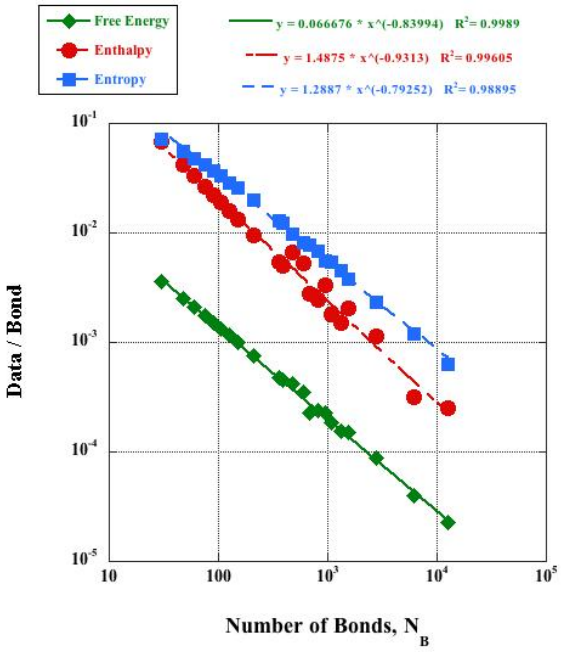

(b) Plots of the free energy, enthalpy, and entropy / bond versus the number of bonds. The data clearly exhibits power law character. This plot uses a standard adjacency matrix.

Figure 2: Power law plots for fullerenes and nanotubes.

Structural Motif	ε_i.(kcal/mol)
pp_p^p	19.8
pp_p^h	17.6
pp_h^h	10.3
ph_p^p	15.7
ph_p^h	12.4
ph_h^h	7.8
hh_p^p	6.2
hh_p^h	4.7
hh_h^h	1.7

Table 1: Heat of formation parameters for the nine structural motifs [19].

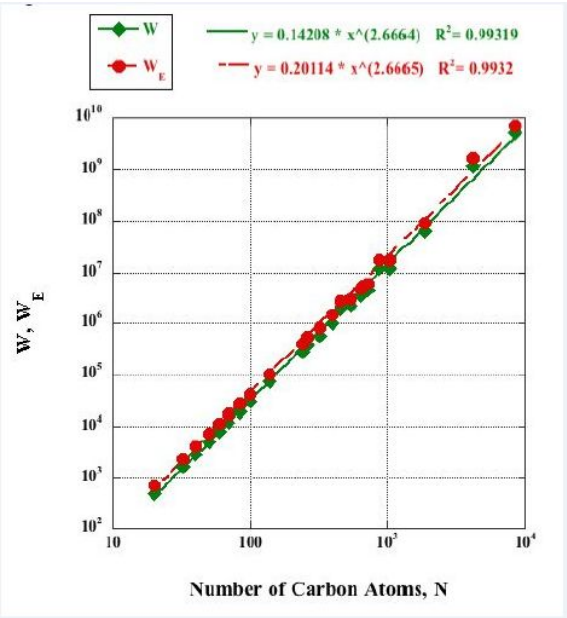

Figure 3: Power law plot of the Wiener Index (standard and Euclidean) for fullerenes and nanotubes versus the number of atoms, N.

of bonds becomes large, we have zero as a limit. Note that the free energy and enthalpy have their signs reversed to allow them to be plotted.

For the fullerenes and nanotubes, we can calculate the energy of formation based on the types of bonds [19] in the structures, see Table 1. We use three types of bonds, as hh, hp, and pp, indicating hexagonal or pentagonal edges, and then further subdivided as to whether the opposite ends of the bond meets a hexagonal or pentagonal cycle. This gives a total of nine bonds and the heat of formation can be calculated as:

$$\Delta H_f = \sum_{i}^{motifs} \varepsilon_i n_i$$

where ε_i is the energy contribution of each structural motif (nine) and n_i is the number of bonds associated with that motif. Since fullerenes have been analyzed extensively [20-22], we show ΔH_f versus length in Angstroms for two of the more common nanotubes, the (5,5) and (10,10) armchair varieties. For nanotubes, the heat of formation includes the energy to create the cap and then the length of the tube. We plot these results in Figure 3. The (5,5) nanotubes contain a cap of C_{60} which has 60 ph_h^h bonds and 30 hh_p^p bonds to give $\Delta H_f = 654$ kcal/mol. As the length of the nanotube increases, we add hh_h^h bonds at 1.7 kcal/mol for each bond. The (10,10) nanotubes have a cap of C_{240} (see Figure 1B) [9], which has 60 ph_h^h bonds, 60 hh_p^h bonds, and 240 hh_h^h bonds, to give $\Delta H_j = 1158$ kcal/mol. Again, as the length of the nanotube increases, we add hh_h^h bonds at 1.7 kcal/mol for each bond. From the graph, we see that since the (10,10) tube is larger, the slope is 41.63 kcal/mol per Å length versus 20.689 kcal/mol per Å length for the (5,5) nanotube. For the (10,10) nanotubes, this gives a cap energy of 64 eV and a length energy of 1.8 eV / Å. These data are in good agreement [9] (40 eV and 0.74 eV / Å) with estimated measurements.

Since we are using a graph-theoretical language, we also calculate the Wiener index for fullerenes and nanotubes, based on the coordinate information in MATLAB. We note that for fullerenes, the Wiener index of $C_{60}(Ih) = 8340$ has been known since 1992 [23], and since then some additional results have been calculated [24-26]. The Wiener index for armchair and zigzag nanotubes has been known since 2004 [27,28]. In Table 2, we list some of the Wiener indices for the fullerenes we investigate, and also the (5,5) and (10,10) nanotubes. The Wiener Index for the fullerenes up to C_{84} agree with previous [24] results, and we add new results up to C720 and also the Euclidean indices for all nanocarbons. In Figure 4, we plot the Wiener index versus N, the number of carbon atoms, to give a power law relationship. We note that for the fullerenes, the Wiener index depends on the structure, so each isomer has a different value for the index. Also, for the nanotubes, the original calculation [27,28] of the Wiener Index did not include caps on the ends, so a direct comparison is not possible. Our modeling is for nanotubes up to 500 Å in length, with caps at both ends.

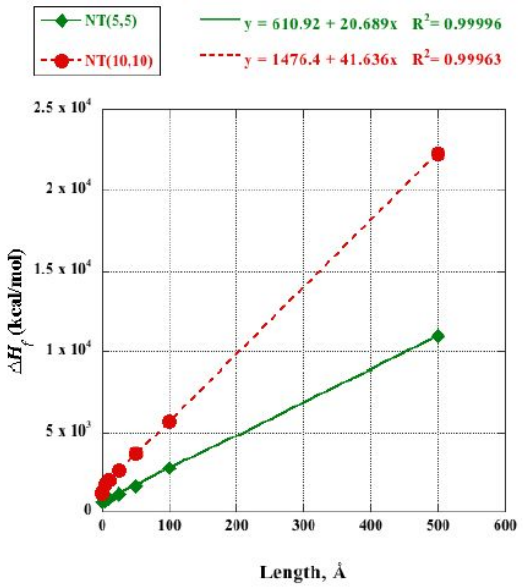

Figure 4: Heat of formation for (5,5) and (10,10) armchair nanotubes versus length in Angstroms.

N	N_B	Nanostruct	Wiener Index (W)	Euclid. Wiener Ind. (W_E)	Ave Bond (Å)
20	30	$C_{20}(I_h)$	500	710.02423	1.4200
32	48	$C_{32}(D_{3d})$	1696	2408.3699	1.4200
40	60	$C_{40}(T_d)$	3000	4260.0679	1.4200
50	75	$C_{50}(D_3)$	5275	7490.6239	1.4200
60	90	$C_{60}(I_h)$	8340	11917.75156	1.4320
70	105	$C_{70}(D_{5h})$	12375	17672.68417	1.4307
84	126	$C_{84}(D_2)$	19646	28041.35179	1.4303
240	360	C_{240}	277440	392329.2316	1.4187
540	810	C_{540}	2119320	2994979.407	1.4190
720	1080	C_{720}	4352340	6162553.116	1.4207
100	150	(5,5)5	30580	42310.62308	1.3879
140	210	(5,5)10	72860	101743.2403	1.3962
260	390	(5,5)25	383700	541217.5044	1.4059
460	690	(5,5)50	1899100	2689448.448	1.4107
880	1320	(5,5)100	12350940	17526597.26	1.4150
4120	6180	(5,5)500	1186916820	1685572294.8	1.4164
320	480	(10,10) 5	569680	804021.9498	1.4156
400	600	(10,10) 10	997120	1410161.755	1.4165
640	960	(10,10) 25	3341840	4737709.644	1.4178
1040	1560	(10,10) 50	12327040	17496098.43	1.4193
1860	2790	(10,10) 100	62759375	89129458.54	1.4187
8360	12540	(10,10) 500	5046069000	7169083944.2	1.4199

Table 2: N is the number of atoms in the nanostructure, fullerenes are denoted by C_N and nanotubes by their chiral indices followed by their length in Angstroms. The topological Wiener Index is W, and the Euclidean Wiener Index is W_E. The bond length is in Angstroms.

4 Conclusion

In summary, we have determined the power law behavior of the free energy, enthalpy, entropy, and atomic displacement of nanocarbons consisting of 20-8360 atoms. We use atomic coordinates to calculate the Wiener index for fullerenes and nanotubes. There are some minor distinctions when using the Euclidean Wiener index, which we have included for completeness. The heat of formation of nanotubes follows a linear relationship with length in agreement with known data.

We have outlined procedures applicable to modeling finite carbon nanostructures using only the 3D coordinates of the structures. These methods will allow others to investigate similar types of models and we encourage the understanding of nano-geometries as we move into the 21st century.

References

[1] Kroto, H.W.; Heath, J.R.; O'Brien, S.C.; Curl, R.F. Smalley, R.E. Nature **318**, 162-163 (1985)
[2] Iijima, S. Nature **354**, 56-58 (1991)
[3] Novoselov, K.S.; Geim, A.K.; Morozov, S.V.; Jiang, D.; Zhang,Y.; Dubonos, S.V.; Grigorieva,I.V.; Firsov, A.A. Science **306**, 666-669 (2004)
[4] Rodriguez-Fortea, A., Alegret, N., Balch, A.L., Poblet, J.M., Nat. Chem. **2**, 955-961 (2010)
[5] Deza, M., Fowler, P.W., Rassat, A., Rogers, K.M., J. Chem. Inf. Comput. Sci. **40**, 550-558 (2000)
[6] Dutour Sikiric, M., Knor, M., Potocnik, P., Siran, J., Skrekovski, R., Discret. Math. **312**, 729-736 (2012)
[7] Beer, F., Gugel, A., Martin, K., Rader, J., Mullen, K., J. Mater. Chem. **7**(8), 1327-1330 (1997)
[8] Baker, R.T.K., Carbon **27**, 315-327 (1989)
[9] Thess, A. et al. Science **273**, 483-487 (1996)
[10] Jin, C.; Suenaga, K.; Iijima, S. ACS Nano, **2**(6), 1275-1279 (2008)
[11] Dresselhaus, M.S.; Eklund, P.C. Adv. Phys., **49**(6), 705-814 (2000)
[12] Estrada, E.; Hatano., N. Chem. Phys. Lett., **486**, 166-170 (2010)
[13] Nikolic, S.; Trinajstic, N.; Mihalic, Z.; Carter, S. Chem. Phys. Lett., **179**, 21-28 (1991)
[14] Vodopivec, A.; Kaatz, F.H.; Mohar, B. J. Math. Chem., **47**, 1145-1153 (2010)
[15] Estrada,E.; Hatano, N. Chem. Phys. Lett., **439**, 247-251 (2007)
[16] Kaatz, F.H.; Estrada, E.; Bultheel, A.; Sharrock, N. Physica A, **391**, 2957-2963 (2012)
[17] Wiener, H. J. Am. Chem. Soc. **69**, 17-20 (1947)
[18] Clauset, A.; Shalizi, C.R.; Newman, M.E.J. SIAM Rev., **51**, 661-703 (2009)
[19] Alcami, M.; Sanchez, G.; Diaz-Tendero, S.; Wang, Y.; Martin, F. J. Nanosci. Nantechnol., **7**, 1329-1338 (2007)
[20] Rojas, A.; Marinez, M.; Amador, P.; Torres, L.A. J. Phys. Chem. B, **111**, 9031-9035 (2007)
[21] Cioslowski, J.; Rao, N.; Moncrieff, D. J. Am. Chem. Soc., **122**, 8265-8270 (2000)
[22] Lair, S.L.; Herndon, W.C.; Murr, L.E.; Quinones, S.A. Carbon, **44**, 447-455 (2006)
[23] Ori, O.; D'Mello, M. Chem. Phys. Lett., **197**, 49-54 (1992)
[24] Balasubramanian, K. J. Phys. Chem., **99**, 10785-10796 (1995)
[25] Babic, D.; Klein, D.J.; Lukovits, I.; Nikolic, S.; Trinajstic, N. Internat. J. Quantum Chem., **90**, 166-176 (2002)
[26] Fowler, P.W. Croatica Chem. Acta, **75**(2), 401-408 (2002)
[27] John, P.E.; Diudea, M.V. Croatica Chem. Acta, **77**(1-2), 127-132 (2004)
[28] Diudea, M.V.; Stefu, M.; Parv, B.; John, P.E. Croatica Chem. Acta, **77**(1-2) 111-115 (2004)